Nuclear Physics B334 (1990) 527–558
North-Holland

QED – A LATTICE INVESTIGATION OF THE CHIRAL PHASE TRANSITION AND THE NATURE OF THE CONTINUUM LIMIT

M. GÖCKELER[1,2], R. HORSLEY[3,4], E. LAERMANN[2,5], P. RAKOW[6], G. SCHIERHOLZ[2,6], R. SOMMER[5] and U.-J. WIESE[2]

[1]*Institut für Theoretische Physik, RWTH Aachen, Sommerfeldstraße, D-5100 Aachen, FRG*
[2]*Gruppe Theorie der Elementarteilchen, Höchstleistungsrechenzentrum HLRZ, c/o KFA, Postfach 1913, D-5170 Jülich, FRG*
[3]*Fachbereich Physik, Universität Kaiserslautern, Postfach 3049, D-6750 Kaiserslautern, FRG*
[4]*Institut für Theoretische Physik, Universität Heidelberg, Philosophenweg 16, D-6900 Heidelberg, FRG*
[5]*Fachbereich Physik, Gesamthochschule Wuppertal, Gaußstraße 20, D-5600 Wuppertal, FRG*
[6]*Deutsches Elektronen-Synchrotron DESY, Notkestraße 85, D-2000 Hamburg 52, FRG*

Received 17 October 1989

We simulate non-compact QED with light dynamical Kogut–Susskind fermions and in the quenched approximation. In both cases we confirm the existence of a second-order chiral phase transition at strong coupling. Near the critical point the theory is shown to be well described by a gaussian model of non-interacting scalar and pseudoscalar fields. We do not find any support for Miransky scaling. Rather, the critical exponents are consistent with their mean field values.

1. Introduction

It is a long-standing and fundamental question whether QED is a consistent and non-trivial field theory in the continuum limit, i.e. when the cut-off is removed.

There is the suspicion that all theories that are not asymptotically free are trivial. Indeed, from finite-order perturbation theory one would conclude that the renormalized charge of QED vanishes for all values of the bare charge in the continuum limit [1]. This is due to an intrinsic inconsistency of the perturbatively defined theory, known as the Landau pole. These arguments are, however, not convincing as the bare charge is taken to be large, and one expects some change in behavior of the theory in the strong coupling regime.

A consistent continuum limit of QED can exist only if the Callan–Symanzik β function [2] has an ultraviolet stable fixed point. This problem can be studied numerically by lattice gauge theory techniques. On the lattice an ultraviolet stable fixed point corresponds to a point of a second- (or higher-) order phase transition, at which the correlation length diverges. A first indication of the nature of the

0550-3213/90/$03.50

continuum theory can be obtained from the critical exponents of the transition. For a complete understanding one will need to know the renormalized parameters of the action at the fixed point in addition.

In a series of studies Kogut et al. [3–5] have reported evidence for the existence of a continuous chiral phase transition in non-compact massless QED* at strong coupling. The results of the Edinburgh group [8] are also consistent with this picture. Kogut and coworkers went on [3–5, 9] to investigate the scaling behavior of the chiral condensate at the phase transition. They claim a non-trivial scaling law for a small number of fermions in agreement with analytic calculations of the truncated Schwinger–Dyson equation for the fermion propagator [10]. From this they concluded that the continuum theory is an interacting theory of bound states.

In this paper we shall investigate the critical behavior of non-compact QED in greater detail. Our first goal is to determine the critical exponents of the chiral phase transition. In the process we have checked the calculations of Kogut, Dagotto and Kocic [3–5, 9]. We do not find any support for non-trivial scaling behavior. Instead, we find that the theory – with and without light dynamical fermions – can be well described by a gaussian model in the critical region. This suggests that the continuum theory is non-interacting.

As a lattice regularized version of QED we take Kogut–Susskind fermions coupled to a non-compact U(1) gauge field A_μ. The action is $S = S_G + S_F$, where

$$S_G = \frac{\beta}{2} \sum_{x,\,\mu<\nu} \left(A_\mu(x) + A_\nu(x+\mu) - A_\mu(x+\nu) - A_\nu(x) \right)^2, \tag{1.1}$$

$$S_F = -\bar{\chi}_x (M+m)_{xy} \chi_y, \tag{1.2}$$

with

$$M_{xy} = -\tfrac{1}{2} \sum_\mu (-1)^{x_1 + \cdots + x_{\mu-1}} \left[e^{iA_\mu(x)} \delta_{y,\,x+\mu} - e^{-iA_\mu(y)} \delta_{y,\,x-\mu} \right]. \tag{1.3}$$

The partition function reads

$$Z = \int [d\bar{\chi}][d\chi][dA_\mu] e^{-S}. \tag{1.4}$$

The lattice constant has been set equal to 1, and $\beta = 1/e^2$, where e is the bare charge. In the classical continuum limit this action describes four degenerate Dirac

* Compact QED, which at small couplings is identical to ordinary non-compact QED, is known to have a first-order phase transition for the Wilson gauge field action [6] and, therefore, has no consistent continuum limit at strong coupling. For the mixed gauge field action with large negative adjoint coupling, however, see ref. [7].

fermions minimally coupled to a U(1) gauge field. For finite lattice spacings the theory has a chiral U(1) × U(1) symmetry in the limit $m \to 0$, while the SU(4) × SU(4) symmetry is only approximate.

Associated with the chiral U(1) symmetry are two order parameters. One order parameter is the chiral condensate,

$$\langle \bar{\psi}\psi \rangle = \lim_{m \to 0} \lim_{V \to \infty} \langle \bar{\chi}\chi \rangle, \tag{1.5}$$

where $V = L^3 T$ is the space-time volume of the lattice with spatial size L and time extent T. After the Grassmann fields have been integrated out, $\langle \bar{\chi}\chi \rangle$ reads

$$\langle \bar{\chi}\chi \rangle = \frac{1}{Z} \int [\mathrm{d}A_\mu] \frac{1}{V} \mathrm{Tr}(M+m)^{-1} \det(M+m) \mathrm{e}^{-S_G}, \tag{1.6}$$

$$Z = \int [\mathrm{d}A_\mu] \det(M+m) \mathrm{e}^{-S_G}. \tag{1.7}$$

The other order parameter is the mass of the pseudoscalar (PS) Goldstone boson, m_{PS}, in the limit $V \to \infty$ and $m \to 0$. This mass is given by the correlation function

$$C_{PS}(t) = \frac{1}{Z} \int [\mathrm{d}A_\mu] \sum_x \left| (M+m)^{-1}_{0,(x,t)} \right|^2 \det(M+m) \mathrm{e}^{-S_G}$$

$$\overset{t \text{ large}}{\cong} A_{PS} [\mathrm{e}^{-m_{PS} t} + \mathrm{e}^{-m_{PS}(T-t)}]. \tag{1.8}$$

From the β and m dependence of the chiral condensate and the Goldstone boson mass near the critical point one can derive three critical exponents. This has led us to concentrate on these quantities in the present paper.

The remainder of the paper is organized as follows. Sect. 2 deals with the problem of computing the order parameter $\langle \bar{\psi}\psi \rangle$ on a finite lattice. We argue that the extrapolation of $\langle \bar{\chi}\chi \rangle$ to $V = \infty$ and $m = 0$ is most reliably done by the help of the eigenvalue density of the fermion matrix M. In sect. 3 we discuss the effective action and its mean field and gaussian approximations. In sect. 4 we investigate quenched QED. Sect. 5 is devoted to the study of QED with dynamical fermions. We conclude with a summary in sect. 6.

2. $\langle \bar{\chi}\chi \rangle$: Extrapolations and finite-size effects

On a finite lattice spontaneous symmetry breaking cannot occur. As a result $\langle \bar{\chi}\chi \rangle = 0$ at $m = 0$. In order to extrapolate $\langle \bar{\chi}\chi \rangle$ to $V = \infty$ and $m = 0$, one may proceed in two different ways. The standard procedure is to extrapolate from larger values of m, where finite-size effects can be neglected. This usually demands that

one has some knowledge of the m dependence of the chiral condensate. Alternatively, one may start from small masses or directly from the eigenvalues of the fermion matrix M, which is less ambiguous. In this case though one has to worry about finite-size effects. We use both methods. In this section we shall discuss the eigenvalue alternative.

In the following we shall distinguish between the valence mass $\overline{m}$ and the dynamical fermion mass m. We define

$$\langle\bar{\chi}\chi\rangle(\overline{m}, m, V) = \frac{1}{Z}\int [\mathrm{d}A_\mu]\,\frac{1}{V}\mathrm{Tr}(M+\overline{m})^{-1}\det(M+m)\mathrm{e}^{-S_G}, \tag{2.1}$$

i.e. we propagate a fermion of mass $\overline{m}$ through a gauge configuration generated with mass m. This can be written

$$\langle\bar{\chi}\chi\rangle(\overline{m}, m, V) = \int_{-\infty}^{\infty}\mathrm{d}\lambda\,\frac{\rho(\lambda, m, V)}{i\lambda+\overline{m}}, \tag{2.2}$$

where $\rho(\lambda, m, V)$ is the eigenvalue density. In this notation the quenched approximation corresponds to $m=\infty$. We write $\langle\bar{\chi}\chi\rangle(\overline{m}, V) = \langle\bar{\chi}\chi\rangle(\overline{m}, \infty, V)$ and $\rho(\lambda, V) = \rho(\lambda, \infty, V)$. From eq. (2.2) we derive $\langle\bar{\psi}\psi\rangle = \pi\rho(0,0,\infty)$ and $\langle\bar{\psi}\psi\rangle = \pi\rho(0,\infty)$ for the dynamical and quenched cases respectively. For the computation of $\langle\bar{\psi}\psi\rangle$ it has been proven [11] to be useful to introduce the quantities

$$N(\lambda, m, V) = \int_0^\lambda \mathrm{d}\bar{\lambda}\,\rho(\bar{\lambda}, m, V), \tag{2.3}$$

$$N(\lambda, V) = \int_0^\lambda \mathrm{d}\bar{\lambda}\,\rho(\bar{\lambda}, V), \tag{2.4}$$

which count the number of eigenvalues per unit volume between 0 and λ. Assuming that ρ is a simple power series at small λ, we obtain in the limit $V\to\infty$

$$N(\lambda, 0, \infty) = \frac{\lambda}{\pi}\langle\bar{\psi}\psi\rangle + \mathrm{O}(\lambda^2), \tag{2.5}$$

$$N(\lambda, \infty) = \frac{\lambda}{\pi}\langle\bar{\psi}\psi\rangle + \mathrm{O}(\lambda^2). \tag{2.6}$$

This suggests computing the small eigenvalues of M, say the first one hundred. The slope of N at $\lambda = 0$ then gives us $\langle\bar{\psi}\psi\rangle$. If $\langle\bar{\psi}\psi\rangle = 0$, we expect the slope to vanish.

However, we have to be careful about finite-size effects. In QCD the problem of finite-size effects associated with a Goldstone boson has been extensively studied, both on the lattice [12, 13] and in the continuum [14]. Because our model has the same chiral symmetry properties as its counterpart in QCD, it is tempting to apply the results also here. This is justified when the photon, which is a further potential

source of finite-size effects, decouples from the electrically neutral $\bar{\chi}_x\chi_x$. We have numerical evidence that this is the case. Jolicoeur and Morel [12] have shown in the strong coupling limit that

$$\langle\bar{\chi}\chi\rangle(m,m,V)=\langle\bar{\psi}\psi\rangle\frac{I_0'(s)}{I_0(s)}+\mathrm{O}(m), \tag{2.7}$$

where $s=mV\langle\bar{\psi}\psi\rangle$. Generalizing this work to the case of unequal masses, we find

$$\langle\bar{\chi}\chi\rangle(m,V)=\langle\bar{\psi}\psi\rangle\frac{I_0'(s)}{I_0(s)}+\mathrm{O}(m) \tag{2.8}$$

for the quenched approximation and

$$\langle\bar{\chi}\chi\rangle(\bar{m},m,V)=\langle\bar{\chi}\chi\rangle(0,m,\infty)\frac{I_0'(\bar{s})}{I_0(\bar{s})}+\mathrm{O}(\bar{m}) \tag{2.9}$$

in the general case, where $\bar{s}=\bar{m}V\langle\bar{\chi}\chi\rangle(0,m,\infty)$. The derivation of eqs. (2.7)–(2.9) exploits only the chiral $\mathrm{U}(1)\times\mathrm{U}(1)$ symmetry of the action. It can be argued that these expressions hold also beyond the strong coupling limit as long as the symmetry is $\mathrm{U}(1)\times\mathrm{U}(1)$. When the chiral symmetry is restored to $\mathrm{SU}(N)\times\mathrm{SU}(N)$, the analysis of Gasser and Leutwyler [14] applies. For $N=2$ and equal masses they obtain a formula similar to eq. (2.7).

Let us concentrate on the quenched approximation first. The eigenvalue density $\rho(\lambda,V)$ is the discontinuity of $\langle\bar{\chi}\chi\rangle$ across the imaginary axis:

$$\rho(\lambda,V)=\lim_{\epsilon\to 0}\frac{1}{2\pi}\left[\langle\bar{\chi}\chi\rangle(-i\lambda+\epsilon,V)-\langle\bar{\chi}\chi\rangle(-i\lambda-\epsilon,V)\right]. \tag{2.10}$$

The Bessel function $I_0(s)$ has zeroes on the imaginary axis [15], which give rise to poles in $\langle\bar{\chi}\chi\rangle$. This leads us to

$$\rho(\lambda,V)=\sum_i\frac{1}{V}\delta\left[\lambda-\nu_i\left(V\langle\bar{\psi}\psi\rangle\right)^{-1}\right]+\mathrm{O}(\lambda), \tag{2.11}$$

where ν_i are the solutions of $I_0(-i\nu)=0$. The number of zeroes that lie between the real axis and $\mathrm{Im}(s)=(n+\frac{1}{4})\pi$ is n. From eq. (2.11) we derive

$$\begin{aligned}N(\lambda,V)&=\sum_i\frac{1}{V}\Theta\left(\lambda V\langle\bar{\psi}\psi\rangle-\nu_i\right)+\mathrm{O}(\lambda^2)\\&=\left(\frac{\lambda}{\pi}\langle\bar{\psi}\psi\rangle-\frac{1}{4V}\right)\Theta\left(\lambda V\langle\bar{\psi}\psi\rangle-\tfrac{1}{4}\pi\right)+\mathrm{O}(\lambda^2).\end{aligned} \tag{2.12}$$

This tells us that the slope is not V dependent. Finite-size effects associated with the Goldstone boson manifest themselves in a negative intercept. They are easy to trace and to correct for in a single volume calculation. In a given volume the intercepts should be the same for all values of β in the broken phase.

In the full theory, i.e. with dynamical fermions, we proceed in a similar way. Instead of eqs. (2.11) and (2.12) we obtain

$$\rho(\lambda, m, V) = \sum_i \frac{1}{V} \delta\left\{\lambda - \nu_i [V\langle\bar{\chi}\chi\rangle(0, m, \infty)]^{-1}\right\} + O(\lambda), \tag{2.13}$$

$$N(\lambda, m, V) = \left[\frac{\lambda}{\pi}\langle\bar{\chi}\chi\rangle(0, m, \infty) - \frac{1}{4V}\right]\Theta\left[\lambda V\langle\bar{\chi}\chi\rangle(0, m, \infty) - \tfrac{1}{4}\pi\right] + O(\lambda^2), \tag{2.14}$$

where $\langle\bar{\chi}\chi\rangle(0, m, \infty) = \lim_{\overline{m}\to 0} \lim_{V\to\infty}\langle\bar{\chi}\chi\rangle(\overline{m}, m, V)$. In this case the procedure allows us to extrapolate immediately to $V = \infty$ and $\overline{m} = 0$, while the extrapolation to $m = 0$ remains to be done. The idea is that $\langle\bar{\chi}\chi\rangle(0, m, \infty)$ is much closer to $\langle\bar{\psi}\psi\rangle$ than $\langle\bar{\chi}\chi\rangle(m, m, V)$ is.

3. Mean field theory and gaussian model

Later on we want to compare our results with the predictions of a non-interacting model. Such a model is the gaussian model, which is a generalization of mean field theory to the extent that it includes gaussian fluctuations.

The gaussian model is obtained from the effective action, which we will derive heuristically now. Following Kawamoto and Smit [16], we first integrate out the gauge fields in eq. (1.4). This leaves us with an expression that depends explicitly only on the Bose fields

$$\mathcal{M}_x = \bar{\chi}_x \chi_x . \tag{3.1}$$

Next we integrate out the Grassmann fields. Replacing the composite Bose fields $\mathcal{M}_x$ by elementary auxiliary Bose fields $\mathcal{M}'_x$, we write

$$Z = \int [\mathrm{d}\mathcal{M}'] \mathrm{e}^{-S_{\mathrm{eff}}(\mathcal{M}')} . \tag{3.2}$$

The effective action has the form

$$S_{\mathrm{eff}}(\mathcal{M}') = -\sum_x m\mathcal{M}'_x + \bar{S}(\mathcal{M}'),$$

$$\bar{S}(\mathcal{M}') = \sum_x \left[c_1 \sum_\mu \mathcal{M}'_x \mathcal{M}'_{x+\mu} + c_2 \left(\sum_\mu \mathcal{M}'_x \mathcal{M}'_{x+\mu} \right)^2 + \cdots \right], \tag{3.3}$$

where the dots include higher non-local contributions. The measure $\mathrm{d}\mathscr{M}'$ has to be chosen appropriately. Under the chiral U(1) × U(1) transformation the Grassmann fields transform as

$$\left.\begin{aligned} \chi_x &\to \mathrm{e}^{i(\delta+\epsilon)}\chi_x \\ \bar{\chi}_x &\to \mathrm{e}^{-i(\delta-\epsilon)}\bar{\chi}_x \end{aligned}\right\} x \text{ even}, \tag{3.4}$$

$$\left.\begin{aligned} \chi_x &\to \mathrm{e}^{i(\delta-\epsilon)}\chi_x \\ \bar{\chi}_x &\to \mathrm{e}^{-i(\delta+\epsilon)}\bar{\chi}_x \end{aligned}\right\} x \text{ odd}, \tag{3.5}$$

which results in

$$\begin{aligned} \mathscr{M}'_x &\to \mathrm{e}^{2i\epsilon}\mathscr{M}'_x \quad x \text{ even}, \\ \mathscr{M}'_x &\to \mathrm{e}^{-2i\epsilon}\mathscr{M}'_x \quad x \text{ odd}. \end{aligned} \tag{3.6}$$

In eq. (3.3) $\bar{S}(\mathscr{M}')$ is invariant under chiral transformations, while the mass term breaks the symmetry down to $\mathrm{U}_\delta(1)$. That is, $S_{\mathrm{eff}}(\mathscr{M}')$ transforms like the original action.

The Bose field $\mathscr{M}'_x$ couples to both scalar (σ) and pseudoscalar (π) particles. We can write

$$\begin{aligned} \mathscr{M}'_x &= \sigma_x + i\pi_x, \quad x \text{ even}, \\ \mathscr{M}'_x &= \sigma_x - i\pi_x, \quad x \text{ odd}. \end{aligned} \tag{3.7}$$

If we insert this into the effective action, we obtain

$$\begin{aligned} S_{\mathrm{eff}}(\sigma,\pi) = \sum_x \Big\{ &\eta\left[(\partial_\mu\sigma_x)^2 + (\partial_\mu\pi_x)^2\right] - m\sigma_x \\ &+ \kappa\left(\sigma_x^2+\pi_x^2\right) + \zeta\left(\sigma_x^2+\pi_x^2\right)^2 + \cdots \Big\}, \end{aligned} \tag{3.8}$$

where we have written only the lowest-order and nearest-neighbor interactions. Note that $\sigma_x^2 + \pi_x^2$ is invariant under chiral transformations. In the following we are interested in the gaussian approximation of eq. (3.8). In order that this makes sense, the coefficients η and ζ must be positive.

Mean field theory assumes that σ_x and π_x are uniformly distributed, i.e. $\sigma_x = \sigma$ and $\pi_x = 0$, so that the chiral condensate σ is given by the minimum of the resulting effective action. If we just consider the lowest contributions, this gives

$$2\kappa\sigma + 4\zeta\sigma^3 - m = 0. \tag{3.9}$$

In the chiral limit, $m \to 0$, $\sigma = \sqrt{-\kappa/2\zeta}$ if κ is negative and $\sigma = 0$ otherwise. A

further essential factor is that one tries to describe critical behavior in terms of analytic effective actions. That means that η, κ and ζ are assumed to be analytic functions of β. Because κ changes sign at the phase transition point, we may write $\kappa = \bar{\kappa}(\beta - \beta_c)$ in the lowest order. This leads to the critical behavior

$$\sigma \propto (\beta_c - \beta)^{1/2}, \qquad \beta_c > \beta. \tag{3.10}$$

The phase transition is of second order. (Generally speaking, this critical exponent arises from all approximations that give a self-consistency relation of the form

$$\sigma = \mathscr{F}(\sigma, \beta), \tag{3.11}$$

where $\mathscr{F}$ is an analytic function that is odd in σ for $m = 0$.) Eq. (3.9) determines furthermore the mass dependence of σ. At the critical point, $\kappa = 0$, for example, one finds

$$\sigma = (m/4\zeta)^{1/3}. \tag{3.12}$$

The gaussian model allows for fluctuations around the minimal action configuration. These fluctuations are treated as independent modes with gaussian distribution. If we insert $\sigma_x = \sigma + \hat{\sigma}_x$ and $\pi_x = 0 + \hat{\pi}_x$ into eq. (3.8), we obtain, in this approximation,

$$S_{\text{eff}}(\sigma, \pi) = \sum_x \Big\{ \eta \Big[(\partial_\mu \hat{\sigma}_x)^2 + (\partial_\mu \hat{\pi}_x)^2 \Big] + (\kappa + 6\zeta\sigma^2)\hat{\sigma}_x^2 + (\kappa + 2\zeta\sigma^2)\hat{\pi}_x^2 - m\sigma + \kappa\sigma^2 + \zeta\sigma^4 \Big\}. \tag{3.13}$$

From eq. (3.13) we can immediately read off the mass of the Goldstone boson [17]:

$$m_{\text{PS}}^2 = \frac{\kappa + 2\zeta\sigma^2}{\eta}. \tag{3.14}$$

If we combine this with eq. (3.9), we obtain

$$m_{\text{PS}}^2 \sigma = m/2\eta. \tag{3.15}$$

In the broken phase eq. (3.15) implies that $m_{\text{PS}}^2 \propto m$ as $m \to 0$. In the symmetric phase m_{PS} does not have to vanish as $m \to 0$. At $m = 0$ eq. (3.14) gives

$$m_{\text{PS}} = \sqrt{\frac{\kappa}{\eta}} \propto (\beta - \beta_c)^{1/2}. \tag{3.16}$$

Similarly, for the mass of the scalar boson, m_S, we obtain

$$m_S^2 = \frac{\kappa + 6\zeta\sigma^2}{\eta} . \tag{3.17}$$

At $m = 0$ this gives

$$m_S = \sqrt{-\frac{2\kappa}{\eta}} \propto (\beta_c - \beta)^{1/2}, \quad \text{for } \beta_c > \beta , \tag{3.18}$$

$$m_S = \sqrt{\frac{\kappa}{\eta}} \propto (\beta - \beta_c)^{1/2}, \quad \text{for } \beta > \beta_c . \tag{3.19}$$

Eqs. (3.10), (3.12), (3.16), (3.18) and (3.19) imply that $\beta = \frac{1}{2}$, $\delta = 3$ and $\nu = \frac{1}{2}$, which are the standard critical exponents of a gaussian model [17].

A first-order chiral phase transition would require a σ^6 term in the effective action.

4. Quenched QED

We shall consider the case of quenched QED first. This case comes closest to the approximate analytic calculations of Miransky [10], on the basis of which it has been claimed that a new source of coupling constant renormalization leads to a fixed point with non-trivial scaling behavior.

Kogut and coworkers [3–5, 9] have searched for Miransky scaling, both in the quenched approximation and in the theory with light dynamical fermions. They find the support for Miransky scaling to be strongest in quenched QED.

4.1. $\langle \bar{\psi}\psi \rangle$

We have performed calculations on 8^4, 12^4 and 16^4 lattices at various values of β using a heat bath algorithm. We use periodic boundary conditions for the gauge fields and antiperiodic fermionic boundary conditions. The chiral condensate $\langle \bar{\psi}\psi \rangle$ is computed from the slope of $N(\lambda, V)$ at $\lambda = 0$. The eigenvalues are obtained by the Lanczos method [18]. For our purposes it is sufficient to know the lowest O(100) eigenvalues. The computations have been done typically on O(50) independent gauge field configurations.

In figs. 1 and 2 we show $N(\lambda, V)V$ for the larger lattices. For $\beta < 0.25$ we find a clear signal for chiral symmetry breaking (fig. 1). At these values of β, $N(\lambda, V)$ is well described by a straight line in the regime of small eigenvalues. The intercepts of $N(\lambda, V)V$ are consistently negative. Thus, the finite-size effects are accounted for by eqs. (2.8) and (2.12), and it appears that the photon does not introduce any new

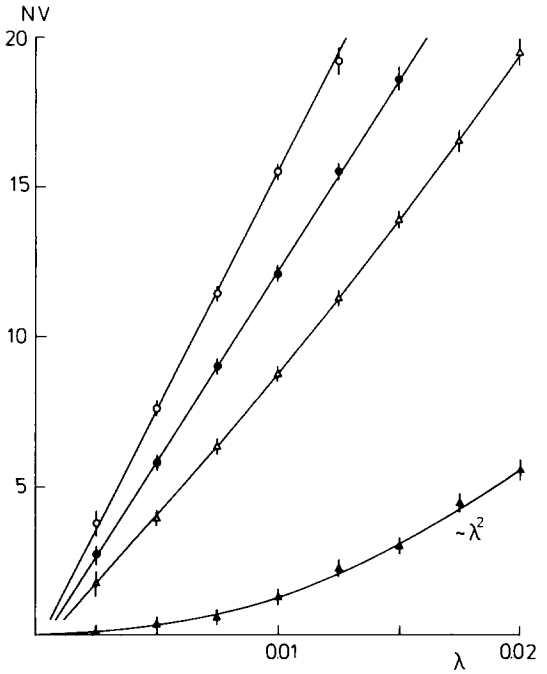

Fig. 1. $N(\lambda, V)/V$ as a function of λ for quenched QED on the 12^4 lattice at $\beta = 0.22$ (○), 0.23 (●), 0.24 (△) and 0.27 (▲). The curves through the data points at $\beta = 0.22$, 0.23 and 0.24 are linear plus quadratic fits. The curve through the data points at $\beta = 0.27$ is a λ^2 fit.

form of the volume dependence of $\langle \bar{\chi}\chi \rangle$. For $\beta > 0.25$, on the other hand, the linear term disappears, and $N(\lambda, V)$ shows a λ^2 behavior for small eigenvalues (figs. 1 and 2). We conclude that chiral symmetry is restored in this region. The situation is slightly more complicated at $\beta = 0.25$. Here we find that $N(\lambda, V)$ can be well fitted by a linear plus quadratic curve (fig. 2), which gives a non-vanishing $\langle \bar{\psi}\psi \rangle$. This result is supported by the fact that we see finite-size effects typical for the broken phase. We noticed, however, that $N(\lambda, V)$ can also be well fitted by a $\lambda^{4/3}$ curve, which would give $\langle \bar{\psi}\psi \rangle = 0$. We will discuss this point further below.

We fit $N(\lambda, V)$ by a linear plus quadratic curve. The upper limit of λ has been chosen such that the fits are stable. It varies from 0.035 on the 8^4 lattice to 0.01 on the 16^4 lattice at $\beta = 0.26$. For $\beta \geqslant 0.26$ we find the slope always to be zero within very small errors. The results are listed in table 1. We find good agreement between our results on the 8^4, 12^4 and 16^4 lattices where they overlap, which is what we expect on the grounds of eq. (2.12). In fig. 3 we plot $\langle \bar{\psi}\psi \rangle$ and in fig. 4 $\langle \bar{\psi}\psi \rangle^2$ as a function of β. The β dependence of $\langle \bar{\psi}\psi \rangle^2$ is very well described by a straight line near the phase transition point. From this we deduce that

$$\langle \bar{\psi}\psi \rangle \propto (\beta_c - \beta)^{1/2} \tag{4.1}$$

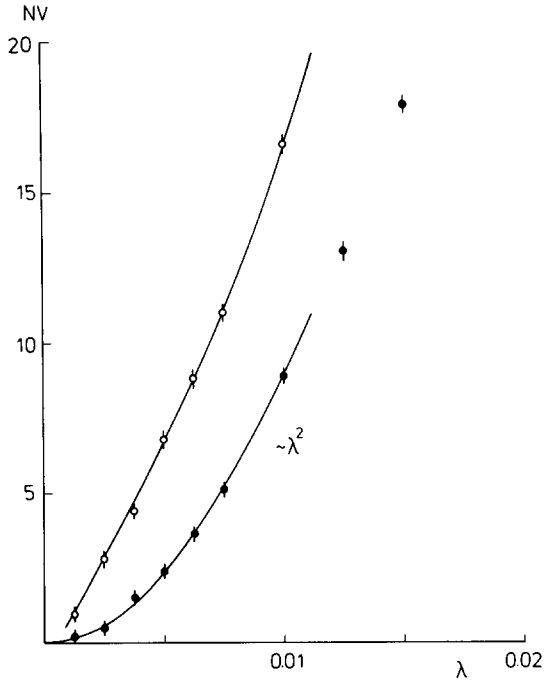

Fig. 2. $N(\lambda, V)V$ as a function of λ for quenched QED on the 16^4 lattice at $\beta = 0.25$ (○) and 0.26 (●). The curve through the data points at $\beta = 0.25$ is a linear plus quadratic fit. The curve through the data points at $\beta = 0.26$ is a λ^2 fit.

TABLE 1

$\langle\bar{\psi}\psi\rangle$ for quenched QED for various values of β on the 8^4, 12^4 and 16^4 lattice. The numbers are obtained from the eigenvalue density of the fermion matrix M

β	8^4	12^4	16^4
0.15	0.494(18)		
0.19	0.356(7)		
0.21	0.276(6)		
0.22	0.239(6)	0.236(5)	
0.23	0.202(8)	0.194(6)	
0.24		0.141(9)	
0.25		0.062(9)	0.060(7)
0.26		0.000(6)	0.000(5)
0.27		0.000(3)	0.000(3)

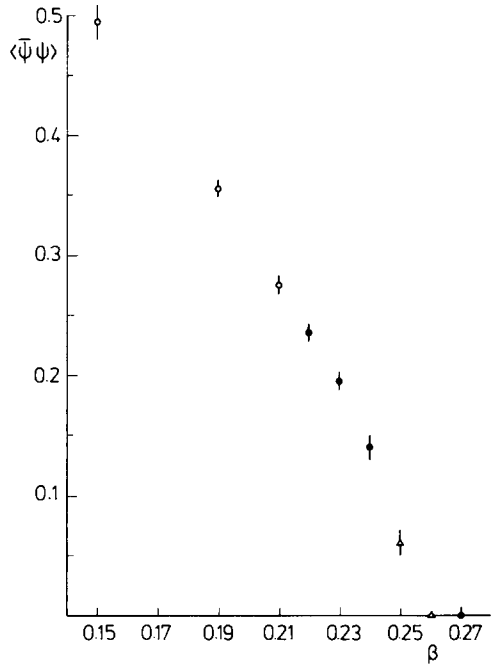

Fig. 3. $\langle\bar{\psi}\psi\rangle$, as found from $N(\lambda, V)$, as a function of β for quenched QED on the 8^4 (○), 12^4 (●) and 16^4 (Δ) lattice.

for $\beta_c \geqslant \beta$. The critical coupling comes out to be $\beta_c \approx 0.252$. Thus, we confirm the occurrence of a second-order chiral phase transition. We find, however, no support for non-trivial scaling behavior. The behavior (4.1) agrees with mean field theory, and that is what we expect for a non-interacting theory.

We can seek a closer connection to mean field theory by fitting $N(\lambda, V)$ with the mean field prediction. We do this by using eq. (2.10), which relates ρ to the discontinuity of $\langle\bar{\chi}\chi\rangle$ for imaginary mass. Solving the mean field equation (3.9) for imaginary mass, where

$$\sigma = \langle\bar{\chi}\chi\rangle(m, \infty), \tag{4.2}$$

we find that the eigenvalue density is given by the positive real solution of

$$(\rho^2 + B)(\rho^2 + B/4)^2 - \lambda^2 A^2 = 0, \tag{4.3}$$

where

$$A = \frac{\sqrt{27}}{2^5\pi^3}\frac{1}{\zeta}, \qquad B = \frac{\kappa}{2\zeta}\frac{1}{\pi^2}. \tag{4.4), (4.5}$$

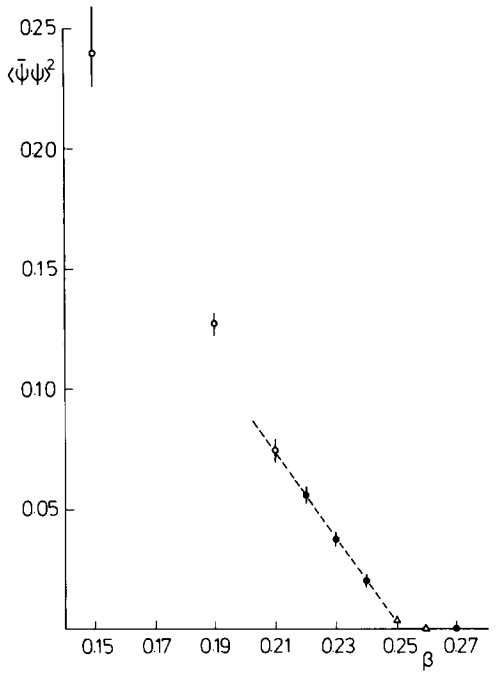

Fig. 4. $\langle\bar{\psi}\psi\rangle^2$, as found from $N(\lambda, V)$, as a function of β for quenched QED on the 8^4 (○), 12^4 (●) and 16^4 (Δ) lattice. The dashed line is a linear fit to the data for $\beta \geqslant 0.21$.

The solutions of eq. (4.3) are shown in the inset of fig. 5. At $\beta = \beta_c$ ($B = 0$) we have $\rho \propto \lambda^{1/3}$ and $N \propto \lambda^{4/3}$, which is, as we noted, a good description of the $\beta = 0.25$ data. In the symmetric phase B is positive and the discontinuity, and therefore ρ, is zero for $\lambda \leqslant \frac{1}{4}B^{3/2}/A$. There is no easy way of taking finite-size effects into account in this approach. Therefore we limit ourselves to the data from the 12^4 and 16^4 lattices and ignore finite-size effects. Fig. 5 shows a fit to our data for N with ρ taken from eq. (4.3). We have parametrized the mean field coefficients as defined in appendix A. The coefficients are allowed to vary quadratically with β. This fit gives $\beta_c = 0.2495(6)$, which is very close to the previously obtained value. The small difference could be due to finite-size effects neglected in the second approach or to the curvature in a ρ proportional to $\lambda^{1/3}$ at $\beta = \beta_c$ not taken into account in the first approach. The $\beta = 0.25$ data is very well described by the predicted $\lambda^{4/3}$ behavior.

4.2. $\langle\bar{\chi}\chi\rangle$ AND MEAN FIELD EXTRAPOLATION

We have computed $\langle\bar{\chi}\chi\rangle(m, V)$ as well. For this purpose we have used a stochastic estimator, which employs one inversion of the fermion matrix for a source vector of random numbers of mean zero. The calculations have been done on

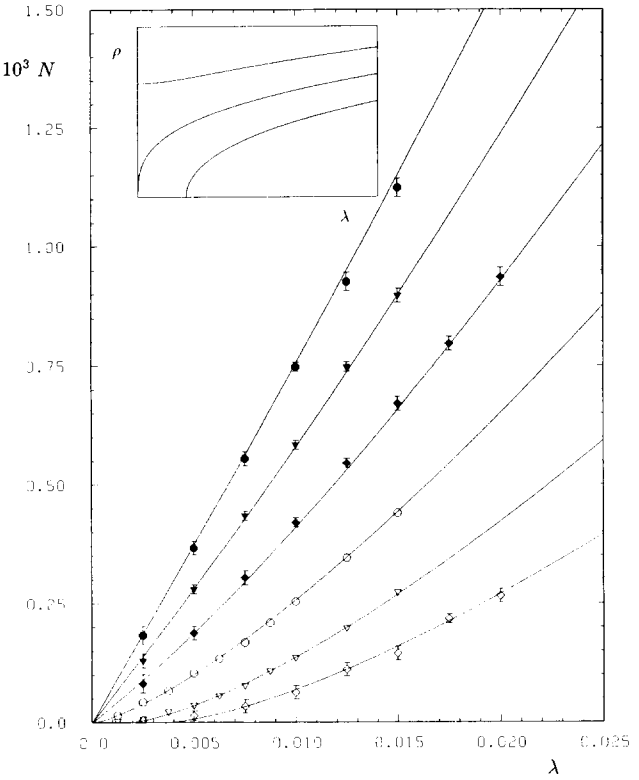

Fig. 5. $N(\lambda, V)$ as a function of λ for quenched QED. The symbols refer to the different values of β: $\beta = 0.22$ (●), 0.23 (▼), 0.24 (◆), 0.25 (○), 0.26 (▽) and 0.27 (◇). The data at $\beta = 0.25$ and 0.26 are taken on 16^4 lattices, the rest on 12^4 lattices. The curves are fits coming from the mean field expression for ρ. The inset shows ρ as given by eq. (4.3) in the broken phase, at the critical point and deep in the symmetric phase. The units are arbitrary. Whenever no error bars are shown, they are smaller than the symbols.

typically O(100) independent gauge field configurations. The β values have been chosen close to the critical value. The results are compiled in table 2. The improvement on previous calculations [4, 9] is that $\langle\bar{\chi}\chi\rangle$ has been computed at up to six different mass values at the various values of β. We do not see any finite-size effects for $V \geqslant 12^4$ and $m \geqslant 0.01$. We take this as further evidence that the photon does not give rise to visible finite-size effects in $\langle\bar{\chi}\chi\rangle$.

The result of the previous section suggests fitting the mass dependence of $\langle\bar{\chi}\chi\rangle$ by mean field theory, identifying $\langle\bar{\chi}\chi\rangle$ with σ. The parametrization of the mean field coefficients is given in appendix A. The fit is based upon the results on the largest lattices. We assume all coefficients to depend linearly on β. The result of the fit is shown in fig. 6. The parameters are given in the first row of table 3. We find that $\langle\bar{\chi}\chi\rangle$ is consistent with mean field behavior. The critical coupling comes

TABLE 2

$\langle\bar{\chi}\chi\rangle(m,V)$ for quenched QED for various values of β and m on the 12^4, 16^4 and 22^4 lattice. We have used a stochastic estimator to compute these numbers

β	m	V	$\langle\bar{\chi}\chi\rangle(m,V)$	β	m	V	$\langle\bar{\chi}\chi\rangle(m,V)$
0.2400	0.002	16^4	0.1467(16)	0.2500	0.010	12^4	0.1353(23)
0.2400	0.010	16^4	0.1717(20)	0.2500	0.020	12^4	0.1749(13)
0.2400	0.040	16^4	0.2521(13)	0.2500	0.002	16^4	0.0773(37)
0.2430	0.020	16^4	0.1975(9)	0.2500	0.004	16^4	0.1012(16)
0.2430	0.040	16^4	0.2477(7)	0.2500	0.010	16^4	0.1361(16)
0.2430	0.010	22^4	0.1634(10)	0.2500	0.020	16^4	0.1768(11)
0.2455	0.010	16^4	0.1534(8)	0.2500	0.030	16^4	0.2021(9)
0.2455	0.040	16^4	0.2387(8)	0.2500	0.040	16^4	0.2261(18)
0.2460	0.004	16^4	0.1183(28)	0.2500	0.002	22^4	0.0819(15)
0.2460	0.010	16^4	0.1464(16)	0.2500	0.004	22^4	0.1004(12)
0.2460	0.040	16^4	0.2381(18)	0.2500	0.010	22^4	0.1354(12)
0.2460	0.004	22^4	0.1199(13)				
0.2460	0.010	22^4	0.1524(9)				
0.2480	0.010	16^4	0.1454(11)				
0.2480	0.020	16^4	0.1830(11)				
0.2480	0.030	16^4	0.2096(13)				
0.2480	0.040	16^4	0.2323(9)				

out to be $\beta_c = 0.2485(2)$, which is slightly smaller than the value obtained from the eigenvalue density.

It is tempting now to fit our data together with the data of Kogut, Dagotto and Kocic [4, 9]. Because of the large span of β values covered by the latter data, we allow the coefficients to vary quadratically with β. The data and the fit are shown in figs. 7 and 8. The parameters are listed in the second row of table 3. We obtain $\beta_c = 0.2482(1)$ in agreement with the fit based on our data alone. The data are surprisingly well described by mean field theory, even quite a distance away from the critical point.

Fig. 8 shows also that $\langle\bar{\chi}\chi\rangle \propto m^{1/3}$ at and near the critical point, as predicted by mean field theory. A linear or quadratic extrapolation of $\langle\bar{\chi}\chi\rangle$ to $m = 0$ is certainly not justified.

The fact, that quenched QED is consistent with mean field theory at the critical point, can be demonstrated further by plotting the quantity $(\beta - \beta_c)/\langle\bar{\chi}\chi\rangle^2$ against $\langle\bar{\chi}\chi\rangle/m^{1/3}$. Near the critical point all data points should fall on one universal curve. This scaling plot is shown in fig. 9 for $\beta_c = 0.2485$. We find good agreement with mean field theory. The nice thing about this plot is that only β_c needs to be taken from a fit. The data from β near β_c are very sensitive to β_c, so this is good evidence that we have located the critical point correctly.

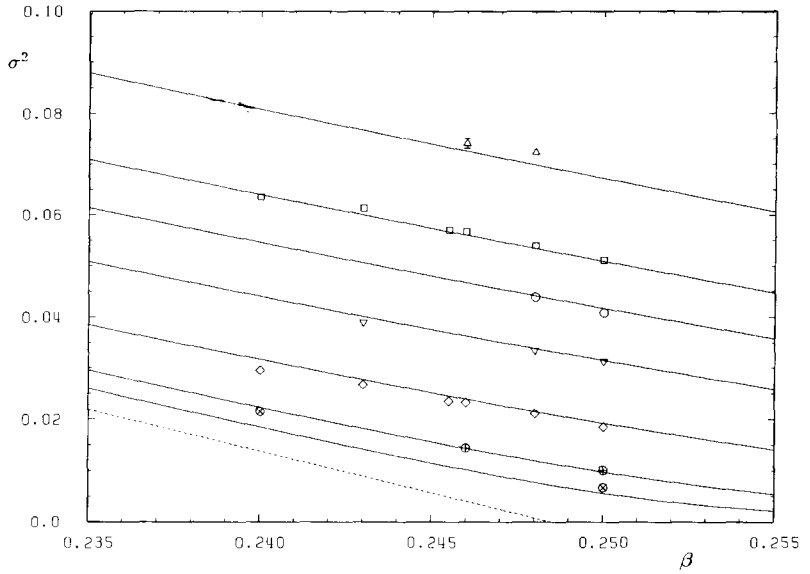

Fig. 6. σ^2 as a function of β for quenched QED. The data of table 2 are compared with a mean field fit. The parameters of the fit are given in the first row of table 3. Whenever we have more than one result for a given value of β and m, that on the largest lattice is shown. The dashed line is the extrapolation to $m = 0$. The symbols refer to the different masses: $m = 0.06$ (△), 0.04 (□), 0.03 (○), 0.02 (▽), 0.01 (◇), 0.004 (⊕) and 0.002 (⊗). Whenever no error bars are shown, they are smaller than the symbols.

TABLE 3
Parameters of the mean field and gaussian model fits to the data. The parameters are defined in appendix A. The first row is a linear fit of σ to the quenched data in table 2. The second row is a quadratic fit of σ to the data in table 2 and the quenched data in ref. [9] combined. The third row shows a linear fit to σ and m_{PS} in dynamical QED. The fourth row shows a linear fit to $\bar{\sigma}$ in dynamical QED. The errors shown are purely statistical

κ_1	κ_2	η_0	η_1	ω_0	ω_1	ω_2	β_c	χ^2/d.f.
−0.81(3)				1.21(1)	1.7(7)		0.2485(2)	8.8
−0.84(1)	−1.32(3)			1.24(1)	0.5(1)	−2.65(28)	0.2482(1)	3.5
−1.42(1)		0.428(2)	−0.88(2)	1.90(1)	−2.8(1)		0.1950(2)	14.7
−1.23(4)				0.37(3)	1.8(3)		0.1948(8)	1.0

5. QED with light dynamical fermions

We shall now investigate QED with one set of dynamical Kogut–Susskind fermions. The calculations are done on 8^4 and 12^4 lattices for fermion masses between 0.02 and 0.16 at various values of β. We have used the hybrid Monte Carlo algorithm [19] for generating the gauge field configurations.

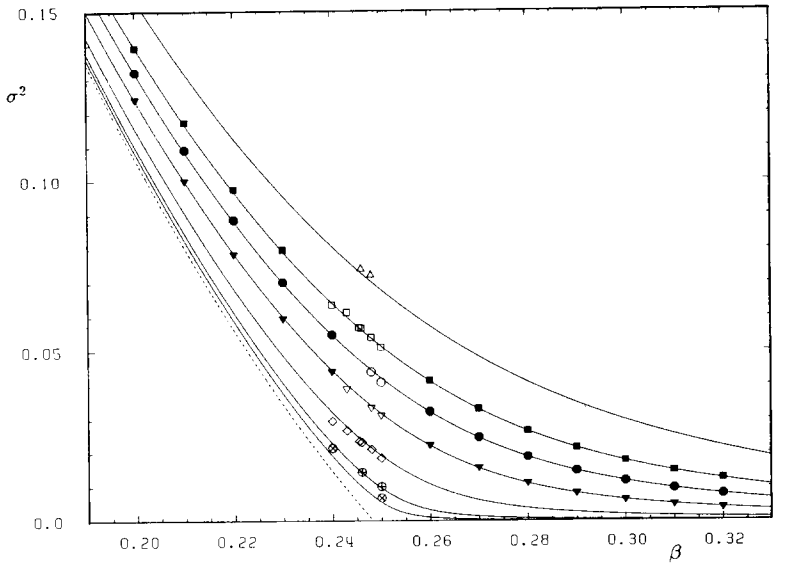

Fig. 7. σ^2 as a function of β for quenched QED. We compare the combined set of quenched data given by our calculations in table 2 and those of Dagotto et al. [9] with a mean field fit. The parameters of the fit are given in the second row of table 3. The open symbols are the same as in fig. 6. A solid symbol indicates the data from ref. [9]. The dashed line is the extrapolation to $m = 0$.

5.1. THE HYBRID MONTE CARLO ALGORITHM

The hybrid Monte Carlo algorithm is exact, but unlike other exact algorithms it is fast enough to be used on larger lattices [20]. It has only one possible source of error, and that is due to incomplete convergence of the fermion matrix inversion. We use the conjugate gradient algorithm without preconditioning for that purpose. The stopping parameter per site is taken to be $r^2 \leqslant 10^{-8}$. In test runs we have checked that increasing the accuracy does not change the fermionic energy. To achieve this, we need on the 8^4 lattice and for $\beta < \beta_c$ between 60 ($m = 0.16$) and 350 ($m = 0.02$) conjugate gradient iterations. The precise value is slightly β dependent. For $\beta > \beta_c$ the number of iterations needed is approximately mass independent, reflecting the fact that m_{PS} does not vanish as $m \to 0$. On the 12^4 lattice these numbers increase by 5–8%. The molecular dynamics step size $\delta\tau$ has been adjusted such as to obtain reasonable acceptance rates. On the 8^4 lattice and for $\beta < \beta_c$ we have chosen $\delta\tau$ between 0.04 ($m = 0.16$) and 0.015 ($m = 0.02$), which leads to acceptance rates of 88% and 71%, respectively. We find the adjustments one has to make in order to keep the acceptance rate constant somewhat weaker than asymptotic estimates would suggest [20]. For $\beta > \beta_c$ we can keep $\delta\tau$ at a constant value of 0.04. In order to maintain the same acceptance rate on the 12^4 lattice, the step size has to be lowered approximately by 30%, which is in accord with the anticipated

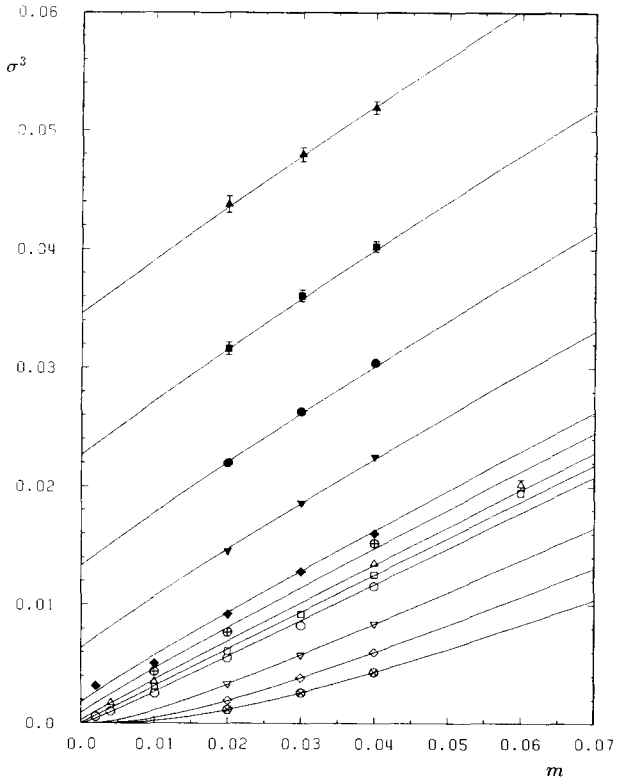

Fig. 8. σ^3 as a function of m for quenched QED. We compare the combined set of quenched data given by our calculations in table 2 and those of Dagotto et al. [9] with a mean field fit. The parameters of the fit are given in the second row of table 3. The symbols refer to different values of β: $\beta = 0.20$ (▲), 0.21 (■), 0.22 (●), 0.23 (▼), 0.24 (◆), 0.243 (⊕), 0.246 (△), 0.248 (□), 0.25 (○), 0.26 (▽), 0.27 (◇) and 0.28 (⊗). The data for $\beta = 0.2455$ are not shown. They coincide with the data for $\beta = 0.246$.

$V^{-1/4}$ behavior. The length of the trajectories has been chosen between 0.35 and 0.70. This results in autocorrelation times of 9 and 2.5, respectively, for Wilson loops up to size $L/2 \times T/2$.

5.2. $\langle\bar{\chi}\chi\rangle(m, m, V)$ AND m_{PS}

Our data sample consists of O(3000) trajectories on the 8^4 lattice and O(1000) trajectories on the 12^4 lattice at each value of β and each mass, starting from equilibrium. Independent configurations are separated by 25 or 50 sweeps. To compute $\langle\bar{\chi}\chi\rangle(m, m, V)$ we have used the stochastic estimator of subsect. 4.2. We compute this quantity every trajectory. We find the autocorrelation time to be significantly smaller than in the case of, e.g. any Wilson loop. The results of the calculation are given in table 4. In order to compute m_{PS}, we use the conjugate gradient algorithm to invert the fermion matrix. This is done on the independent

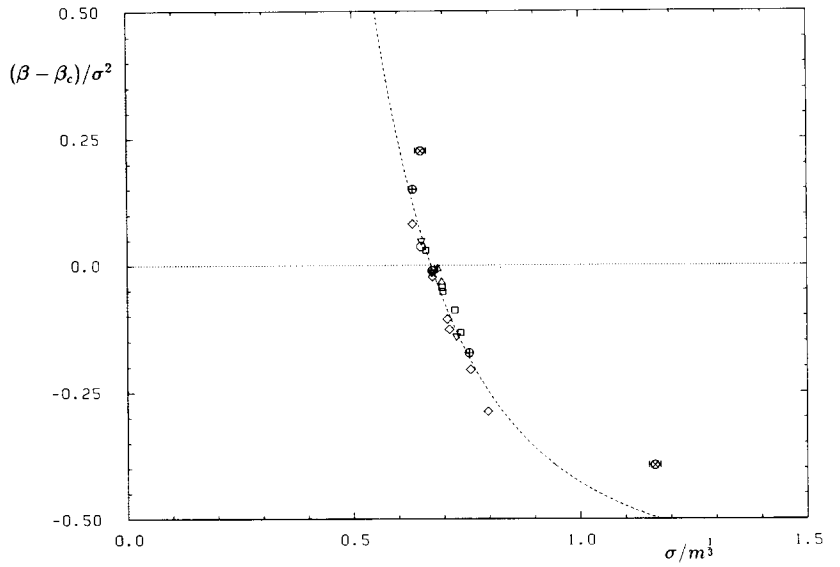

Fig. 9. Scaling plot of $(\beta-\beta_c)/\sigma^2$ versus $\sigma/m^{1/3}$ for $\beta_c = 0.2485$ for quenched QED. This β_c value is taken from the mean field fit in the first row of table 3. If the critical indices have mean field values, all data taken near the phase transition should lie on a universal curve. The mass values of the data are indicated by the same symbols as in fig. 6. The dashed curve is the expected curve according to the fit in the first row of table 3. The two sites that lie furthest from the curve are those for $m = 0.002$, which is our smallest mass value.

configurations and for up to three well-separated source points. Typical examples of the correlation function are shown in figs. 10 and 11. We fit $C_{PS}(t)$ for $1 \leqslant t \leqslant T-1$ by a single mass term. There is no sign of an excited state beyond $t = 1$, as can be seen in figs. 10 and 11, nor is there any sign of a continuum. Chiral symmetry says that at $m = 0$ the Goldstone boson cannot decay into photons (the lattice U(1) does not have the anomaly responsible for the decay of the physical π^0). The other possible continuum contribution comes from the decay to two fermions when energetically allowed. The absence of the continuum is perhaps a hint that the renormalized fermion mass is large. The pseudoscalar masses are collected in table 4.

The chiral condensate $\langle\bar{\chi}\chi\rangle(m, m, V)$ and the correlation function $C_{PS}(t)$ are related by the Ward identity

$$\langle\bar{\chi}\chi\rangle(m, m, V) = m \sum_{t=0}^{T} C_{PS}(t). \tag{5.1}$$

In the limit $m \to 0$ only the Goldstone boson contributes to eq. (5.1). We may

TABLE 4
$\langle S_G\rangle/(V\beta)$, $\langle\bar\chi\chi\rangle(m,m,V)$, $\langle\bar\chi\chi\rangle_W(m,m,V)$ and m_{PS} for dynamical QED for various values of β and m on the 8^4 and 12^4 lattice. (S_G is the gauge field action)

β	m	$\langle S_G\rangle/(V\beta)$	$\langle\bar\chi\chi\rangle(m,m,V)$	$\langle\bar\chi\chi\rangle_W(m,m,V)$	m_{PS}
			8^4		
0.16	0.02	1.3617(22)	0.3804(16)	0.381(3)	0.360(3)
0.16	0.04	1.3739(11)	0.4062(12)	0.392(2)	0.508(2)
0.16	0.09	1.4018(8)	0.4470(7)	0.460(3)	0.720(3)
0.16	0.16	1.4280(8)	0.4782(5)	0.470(4)	0.941(3)
0.18	0.02	1.1873(20)	0.2790(18)		
0.18	0.04	1.2031(9)	0.3281(11)	0.314(2)	0.543(3)
0.18	0.09	1.2287(8)	0.3907(7)	0.390(3)	0.749(8)
0.18	0.16	1.2583(5)	0.4380(5)	0.436(3)	0.961(4)
0.19	0.02	1.1166(11)	0.2255(15)	0.218(2)	0.447(4)
0.19	0.04	1.1331(13)	0.2850(13)		
0.19	0.09	1.1589(6)	0.3619(6)	0.356(3)	0.768(3)
0.19	0.16	1.1872(6)	0.4172(5)	0.414(3)	0.974(3)
0.20	0.02	1.0592(6)	0.1694(10)	0.163(2)	0.498(8)
0.20	0.04	1.0731(7)	0.2483(18)	0.248(3)	0.583(5)
0.20	0.09	1.0000(7)	0.3361(5)	0.328(3)	0.787(5)
0.20	0.16	1.1244(5)	0.3975(5)	0.395(4)	0.990(4)
0.21	0.09	1.0466(5)	0.3124(5)	0.310(2)	0.804(4)
0.21	0.16	1.0205(5)	0.3798(4)	0.378(2)	0.996(3)
0.22	0.04	0.9771(8)	0.1808(10)	0.185(2)	0.676(7)
0.22	0.09	0.9972(4)	0.2887(5)	0.291(4)	0.824(5)
0.22	0.16	1.0205(5)	0.3618(5)	0.350(3)	1.014(4)
0.23	0.04	0.9357(5)	0.1574(6)	0.157(3)	0.707(9)
0.24	0.04	0.9009(5)	0.1416(7)	0.143(2)	0.726(8)
0.25	0.04	0.8673(5)	0.1255(3)	0.125(1)	0.792(7)
0.26	0.02	0.8342(4)	0.0595(3)	0.060(1)	0.787(13)
0.26	0.04	0.8373(3)	0.1139(4)	0.113(2)	0.812(7)
			12^4		
0.19	0.020	1.1163(8)	0.2298(9)	0.233(3)	0.419(3)
0.19	0.040	1.1320(10)	0.2866(6)	0.284(2)	0.556(4)
0.20	0.020	1.0619(8)	0.1880(8)	0.176(2)	0.454(4)
0.20	0.040	1.0757(7)	0.2535(9)	0.262(5)	0.576(4)
0.20	0.090	1.0998(5)	0.3369(5)	0.341(4)	0.781(4)
0.20	0.160	1.1263(6)	0.3986(2)	0.398(3)	0.987(3)

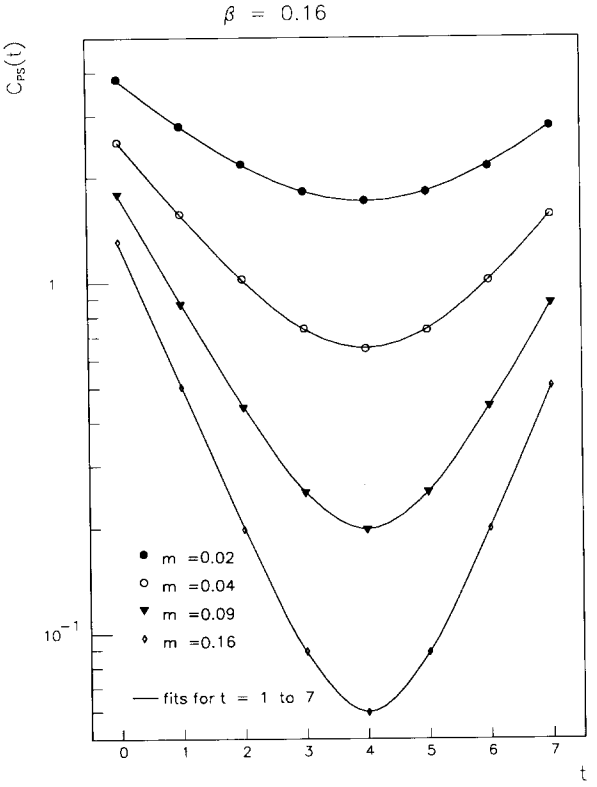

Fig. 10. The pseudoscalar correlation function $C_{PS}(t)$ as a function of t for dynamical QED on the 8^4 lattice in the broken phase at $\beta = 0.16$ and $m = 0.16$ ($\diamond$), 0.09 ($\blacktriangledown$), 0.04 ($\circ$) and 0.02 ($\bullet$). The solid curves are single mass fits to $1 \leqslant t \leqslant 7$. The error bars are smaller than the symbols.

therefore consider

$$\langle \bar{\chi}\chi \rangle_W(m, m, V) = m \sum_{t=0}^{T} A_{PS}(e^{-tm_{PS}} + e^{-(T-t)m_{PS}})$$

$$= mA_{PS} \coth(m_{PS}/2)(1 - e^{-Tm_{PS}}) \qquad (5.2)$$

as an alternative estimator for $\langle \bar{\chi}\chi \rangle$. The results of the calculation are given in table 4. The difference from $\langle \bar{\chi}\chi \rangle(m, m, V)$ is very small. We shall base our further analysis on $\langle \bar{\chi}\chi \rangle(m, m, V)$, because it has the smaller statistical errors.

5.3. $\langle \bar{\chi}\chi \rangle(0, m, \infty)$

In order to compute $\langle \bar{\chi}\chi \rangle(0, m, \infty)$, we proceed in the same way as in sect. 4. The calculations are done on the independent gauge field configurations. In figs. 12 and

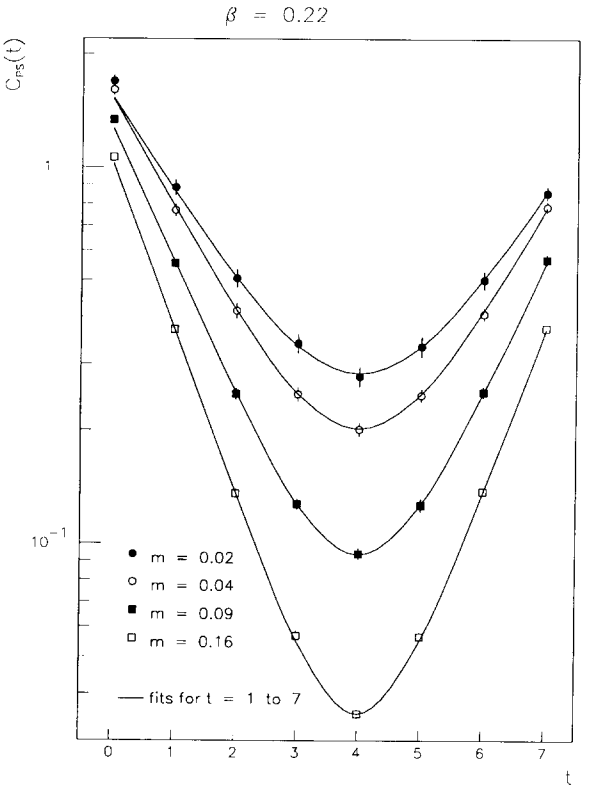

Fig. 11. The pseudoscalar correlation function $C_{PS}(t)$ as a function of t for dynamical QED on the 8^4 lattice in the symmetric phase at $\beta = 0.22$ and $m = 0.16$ (□), 0.09 (■), 0.04 (○) and 0.02 (●). The solid curves are single mass fits to $1 \leqslant t \leqslant 7$.

13 we show $N(\lambda, m, V)V$ for the 12^4 lattice at $\beta = 0.19$ and 0.20, respectively. The phase transition point will turn out to lie between these two values of β. At $\beta = 0.19$ we find that $N(\lambda, m, V)$ can be well approximated by a straight line in the regime of small eigenvalues. At $\beta = 0.20$, on the other hand, $N(\lambda, m, V)$ gets more and more curved with decreasing m. The intercepts of $N(\lambda, m, V)V$ are negative, as we expect on a finite lattice. They are smaller though than in the quenched case (cf. figs. 1 and 2), which indicates that finite-size effects of the kind discussed in sect. 2 are less pronounced here.

We fit $N(\lambda, m, V)$ by a linear plus quadratic curve. The upper limit of λ has been chosen such that the fits are stable. As in the quenched case, $\langle\bar{\chi}\chi\rangle(0, m, \infty)$ is obtained from the slope of the linear term according to eq. (2.14). The results are listed in table 5 and are drawn in fig. 14.

Fig. 14 shows that the extrapolated value $\langle\bar{\chi}\chi\rangle(0, m, \infty)$ is still subject to finite-size effects at $m = 0.02$. This is not surprising. On the 8^4 lattice at $\beta = 0.20$ and $m = 0.02$ we find that there are, on the average, only ≈ 1.5 eigenvalues that are

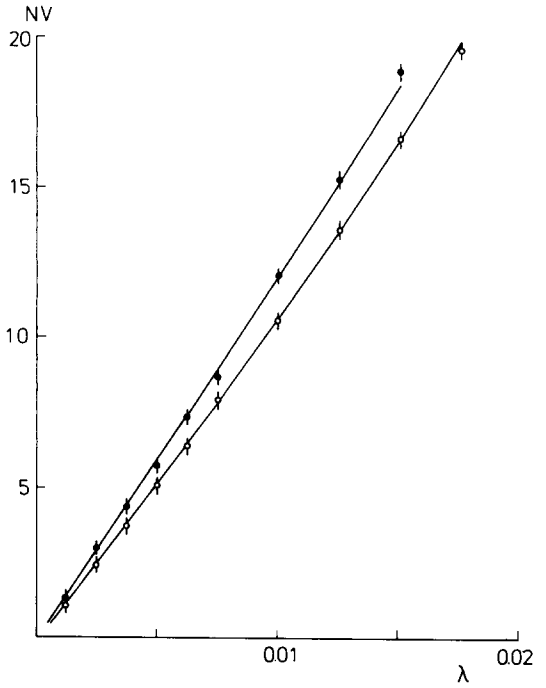

Fig. 12. $N(\lambda, m, V)V$ as a function of λ for dynamical QED on the 12^4 lattice at $\beta = 0.19$ and $m = 0.04$ (●) and 0.02 (○). The curves are linear plus quadratic fits to the data.

smaller than 0.02. Thus, the 8^4 lattice is unable to respond properly to masses $m \leqslant 0.02$. In the following we take the result on the largest lattice for $\langle \bar{\chi}\chi \rangle(0, m, \infty)$.

With more data, especially on larger lattices, it will be interesting to fit N with the behavior of eq. (4.3).

5.4. EXTRAPOLATIONS AND GAUSSIAN MODEL

We shall ask now whether our data can be described by the gaussian model. We have

$$\sigma = \langle \bar{\chi}\chi \rangle(m, m, \infty). \tag{5.3}$$

For the condensate dealt with in subsect. 5.3 we write

$$\bar{\sigma} = \langle \bar{\chi}\chi \rangle(0, m, \infty). \tag{5.4}$$

If the m dependence of σ is given by eq. (3.9), the following relationship holds:

$$2\kappa\bar{\sigma} + 4\zeta\bar{\sigma}^3 = 2\kappa\sigma + 4\zeta\sigma^3 + O(m). \tag{5.5}$$

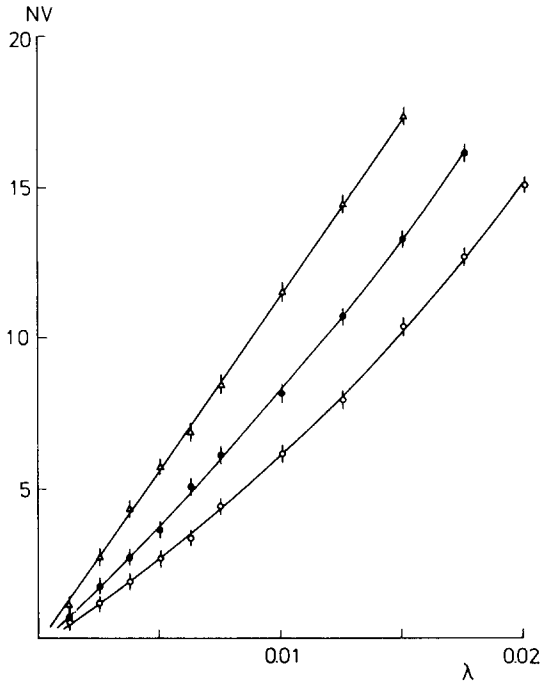

Fig. 13. $N(\lambda, m, V)V$ as a function of λ for dynamical QED on the 12^4 lattice at $\beta = 0.20$ and $m = 0.09$ (Δ), $m = 0.04$ ($\bullet$) and 0.02 ($\circ$). The curves are linear plus quadratic fits to the data.

TABLE 5

$\langle\bar{\chi}\chi\rangle(0, m, \infty)$ for dynamical QED for various values of β and m on the 8^4 and 12^4 lattice. The numbers are obtained from the eigenvalue density of the fermion matrix M

β	m	8^4	12^4	β	m	8^4	12^4
0.16	0.02	0.350(6)		0.20	0.02	0.100(16)	0.078(8)
0.16	0.04	0.362(6)		0.20	0.04	0.118(14)	0.116(8)
0.16	0.09	0.383(6)		0.20	0.09	0.169(12)	0.172(4)
0.16	0.16	0.413(6)		0.20	0.16	0.215(11)	
0.18	0.02	0.235(10)		0.21	0.02		
0.18	0.04	0.258(6)		0.21	0.04		
0.18	0.09	0.295(6)		0.21	0.09	0.086(10)	0.172(4)
0.18	0.16	0.328(9)		0.21	0.16	0.128(8)	
0.19	0.02	0.174(14)	0.157(8)				
0.19	0.04	0.186(12)	0.180(7)				
0.19	0.09	0.227(10)					
0.19	0.16	0.267(10)					

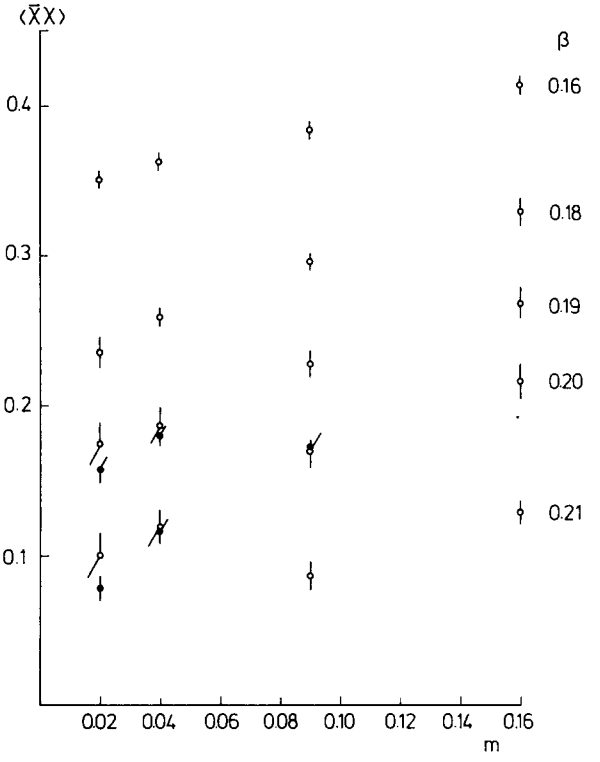

Fig. 14. $\langle\bar{\chi}\chi\rangle(0, m, V)$, as obtained from $N(\lambda, m, V)$, as a function of m for dynamical QED on the 8^4 (○) and 12^4 (●) lattice. Finite-size effects are not large.

This leads to the mean field formula for $\bar{\sigma}$:

$$2\kappa\bar{\sigma} + 4\zeta\bar{\sigma}^3 - \omega m = 0. \tag{5.6}$$

We find that $\omega \ll 1$, which means that the extrapolation to $m = 0$ is much easier.

Let us first consider the quantities σ and m_{PS}. We identify $\langle\bar{\chi}\chi\rangle(m, m, \infty)$ with the value of $\langle\bar{\chi}\chi\rangle(m, m, V)$ on the largest lattice. Near the critical point the β and m dependence of σ and m_{PS} is given by eqs. (3.9) and (3.14) according to the model. We parametrize the coefficients in the effective action as stated in appendix A. All fits in the following figures assume a linear β dependence of these coefficients. In figs. 15–17 we show the simultaneous fit of σ and m_{PS}. The values at $m = 0.16$ are not fitted because they fall obviously outside the range of applicability of eqs. (3.9) and (3.14). They are included in the figure for illustration. The parameters of the fit are listed in the third row of table 3. We find that σ and m_{PS} are well fitted by the gaussian model*: The parameters are mainly fixed by the σ

* Horowitz [21] has made a mean field fit based on the gap equation of a Nambu–Jona-Lasinio model [22] to the Edinburgh data [8] on σ. He finds a good fit too.

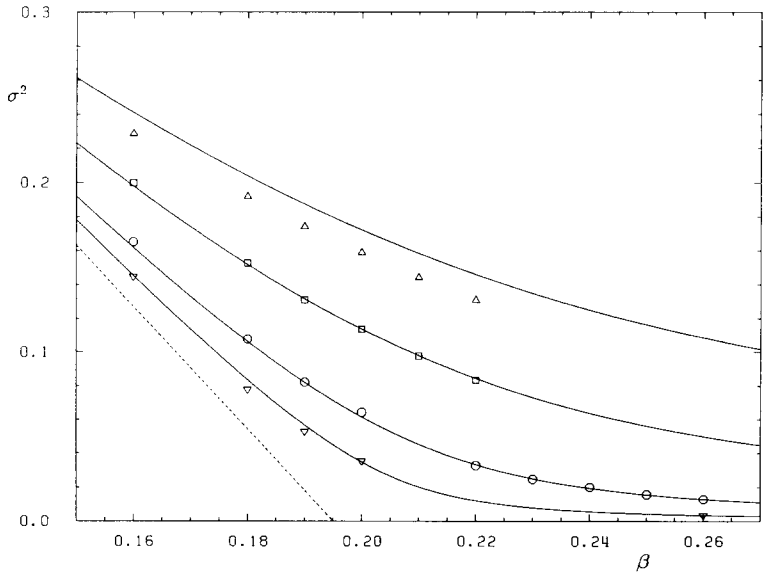

Fig. 15. σ^2 as a function of β for dynamical QED. We compare the data of table 4 with a combined fit to σ and m_{PS}. The parameters of the fit are given in the third row of table 3. The dashed curve is the extrapolation to $m = 0$. The symbols refer to the different masses: $m = 0.16$ (△), 0.09 (□), 0.04 (○) and 0.02 (▽). The fit did not include the data values at $m = 0.16$. All errors are smaller than the symbols.

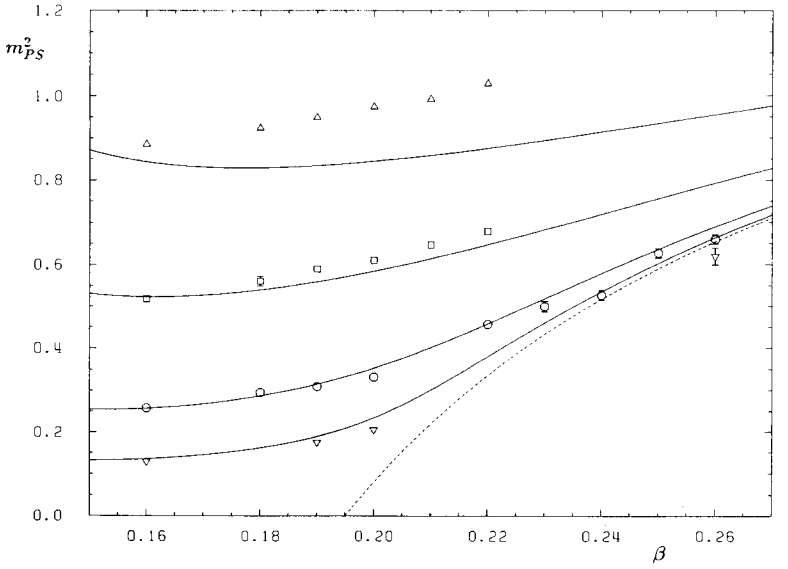

Fig. 16. m^2_{PS} as a function of β for dynamical QED. We compare the data of table 4 with a combined fit to σ and m_{PS}. The parameters of the fit are given in the third row of table 3. The dashed curve is the extrapolation to $m = 0$. The mass values are denoted by the same symbols as in fig. 15. The fit did not include the data values at $m = 0.16$. Whenever no error bars are shown, they are smaller than the symbols.

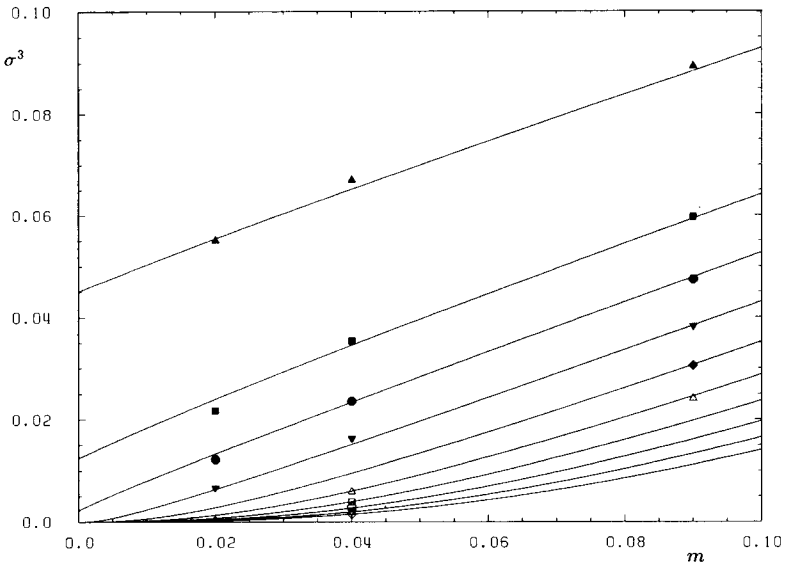

Fig. 17. σ^3 as a function of m for dynamical QED. We compare the data of table 4 with a combined fit to σ and m_{PS}. The parameters of the fit are given in the third row of table 3. The symbols refer to the different values of β: $\beta = 0.16$ (▲), 0.18 (■), 0.19 (●), 0.20 (▼), 0.21 (◆), 0.22 (△), 0.23 (□), 0.24 (○), 0.25 (▽) and 0.26 (◇).

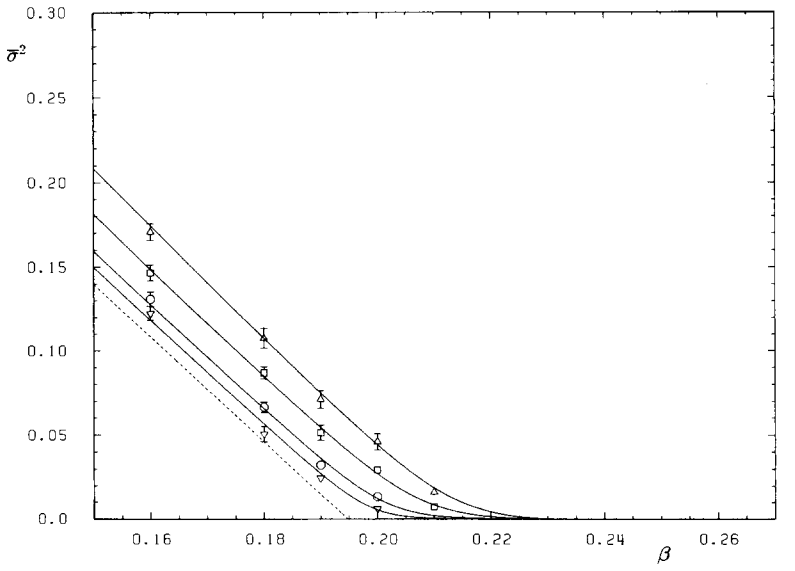

Fig. 18. $\bar{\sigma}^2$ as a function of β for dynamical QED. We compare the data of table 5 with a mean field fit to $\bar{\sigma}$. The parameters of the fit are given in the fourth row of table 3. The dashed curve is the extrapolation to $m = 0$. The symbols are as in fig. 15. Whenever no error bars are shown, they are smaller than the symbols.

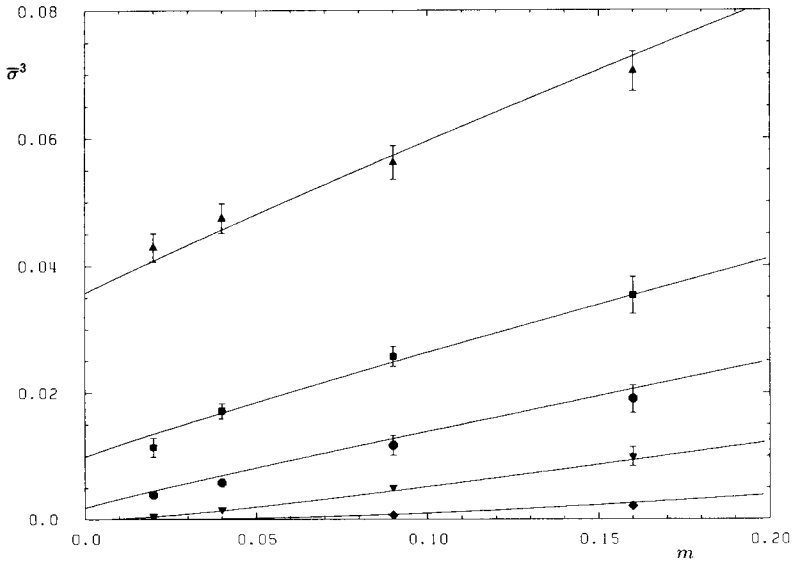

Fig. 19. $\bar{\sigma}^3$ as a function of m for dynamical QED. We compare the data of table 5 with a mean field fit to $\bar{\sigma}$. The parameters of the fit are given in the fourth row of table 3. The β values are denoted by the same symbols as in fig. 17.

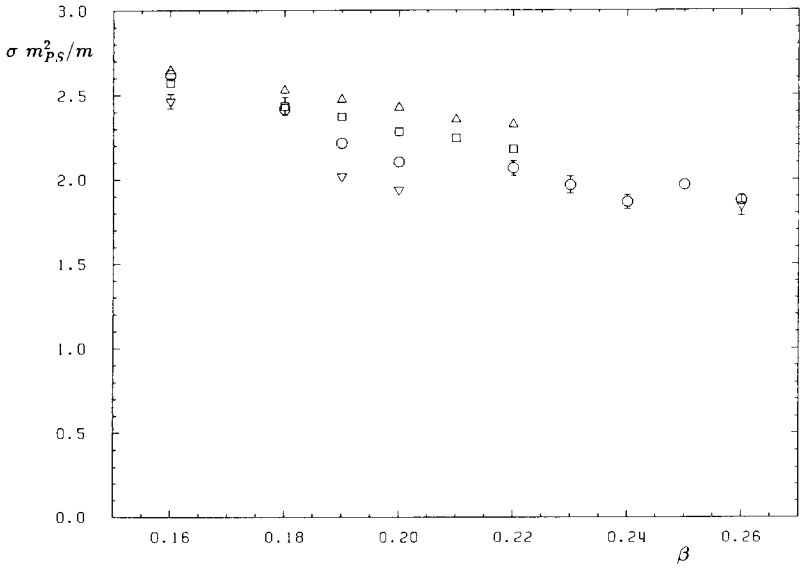

Fig. 20. $\sigma m_{PS}^2/m$ as a function of β for dynamical QED. The mass values are denoted by the same symbols as in fig. 15. The gaussian model predicts that all data should lie on a single curve.

data (because it is so accurate). With the small error bars on σ a χ^2/d.f. of 15 corresponds to a difference between fit and data of only 1%. Much of this seems to arise from the $m = 0.09$ data (a mass value larger than that we could work with in the quenched case). The $m = 0.16$ data shows definite deviation from mean field behavior, which warns us that there are probably also small deviations in the $m = 0.09$ data. The dashed lines in figs. 15 and 16 represent the values extrapolated to $m = 0$. We obtain $\beta_c = 0.1950(2)$. From fig. 17 we can read off, even without a fit, that $\sigma \propto m^{1/3}$ at the critical coupling.

We shall now consider the quantity $\bar{\sigma}$. Its β and m dependence is governed by eq. (5.6), according to mean field theory. The difference from σ is that the mass dependence is somewhat diminished, while the coefficients κ and ζ should be the same. In figs. 18 and 19 we show the fit. The corresponding parameters are given in the fourth row of table 3. We obtain a very good fit in this case as well. Fig. 18 shows that $\bar{\sigma}$ is indeed much closer to $\langle \bar{\psi}\psi \rangle$ (dashed line) than σ was, which does not leave much ambiguity in the extrapolation of the data. We certainly can rule out Miransky scaling [10]. The critical coupling comes out to be $\beta_c = 0.1948(8)$, which coincides with the previous value. Fig. 19 shows that $\bar{\sigma} \propto m^{1/3}$ at the critical coupling all the way up to $m = 0.16$.

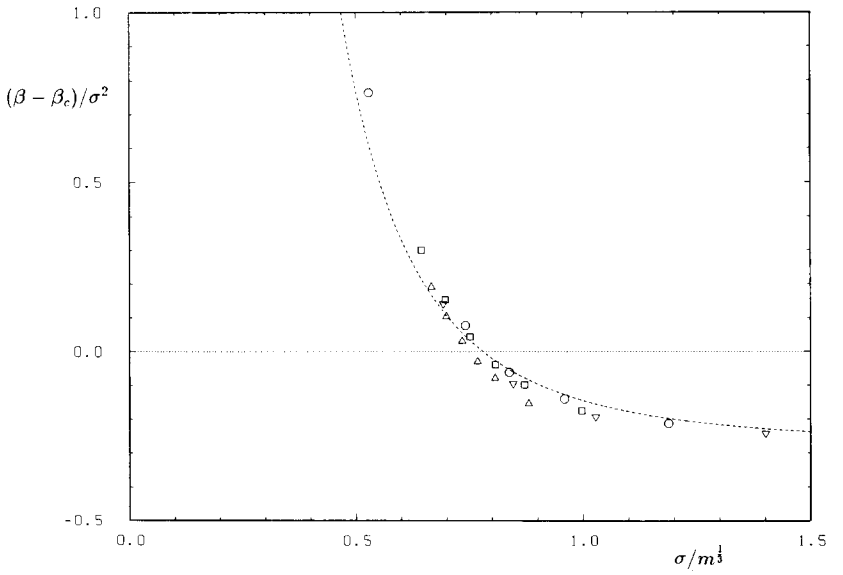

Fig. 21. Scaling plot of $(\beta - \beta_c)/\sigma^2$ versus $\sigma/m^{1/3}$ for $\beta_c = 0.1950$ for dynamical QED. This β_c value is taken from the gaussian model fit in the third row of table 3. If the critical indices have mean field values, all data taken near the phase transition should lie on a universal curve. The mass values of the data are indicated by the same symbols as in fig. 15. The dashed curve is the expected curve according to the fit in the third row of table 3.

A further test of the gaussian model interpretation of the data is provided by the quantity $m_{PS}^2\sigma/m$, which, according to eq. (3.15), should only depend on β. We have plotted this quantity in fig. 20. If one considers that m varies by almost an order of magnitude, the agreement between the data and the predictions of the gaussian model is good. In fig. 21 we have plotted furthermore the quantity $(\beta - \beta_c)/\sigma^2$ versus $\sigma/m^{1/3}$ for $\beta_c = 0.1948$. As in the quenched case, we find that our data scale in agreement with mean field theory.

6. Summary

We have investigated non-compact QED in the quenched approximation and for one set of dynamical Kogut–Susskind fermions. So far we have calculated the chiral condensate and the mass of the Goldstone boson. Particular effort was spent on the extrapolation of our data to the infinite volume and to zero mass. We find evidence for a second-order chiral phase transition. Near the critical point our results agree very well with the predictions of a gaussian model, which is an indication that QED is non-interacting in the continuum limit.

Compared with refs. [4, 5, 9] we find a lower β_c in both quenched and dynamical QED. We see no sign of the essential singularity tail predicted by Miransky [10]. These discrepancies come mainly from the extrapolations to $m = 0$. Before rejecting mean field exponents, one should use mean field theory to extrapolate to $m = 0$. Our graphs of m dependence clearly show mean field behavior, whereas a polynomial fit is certainly ruled out.

Our gaussian model has a chiral U(1) symmetry. In the continuum limit we expect the SU(4) symmetry to be restored, in which case the gaussian model should be extended. It would be desirable to confirm these results on larger lattices and with higher statistics.

Let us now turn to some speculations as to the effective theory at the fixed point. Our mean field fit is based on a σ model, and such a model could be the effective theory one is seeking. It has a U(1) symmetry corresponding to the chiral symmetry of QED. This model can be given a chirally symmetric coupling to the fermion field, leading to a fermion mass proportional to $\langle\bar{\chi}\chi\rangle$ near the critical point. Another model in the same universality class might be the Nambu–Jona-Lasinio model, as was suggested by Horowitz [21].

We would like to thank A.N. Burkitt for helpful discussions. The calculations have been done on the Cray X-MP of the HLRZ. We are grateful for their generous support.

Appendix A

PARAMETRIZATION OF MEAN FIELD FITS

We divide the effective action (3.13) by ζ. The reason for this choice is that $\sigma^2 = -\kappa/2\zeta$ for $\beta < \beta_c$ and $m = 0$. We choose the parametrization:

$$\left.\begin{matrix} 1/\zeta \\ \omega/\zeta \end{matrix}\right\} = \omega_0 + \omega_1\left(1 - \frac{\beta}{\beta_c}\right) + \omega_2\left(1 - \frac{\beta}{\beta_c}\right)^2, \tag{A.1}$$

$$\kappa/\zeta = \kappa_1\left(1 - \frac{\beta}{\beta_c}\right) + \kappa_2\left(1 - \frac{\beta}{\beta_c}\right)^2, \tag{A.2}$$

$$\eta/\zeta = \eta_0 + \eta_1\left(1 - \frac{\beta}{\beta_c}\right), \tag{A.3}$$

where β_c is the critical coupling. The coefficient ω/ζ occurs in the mean field equation (5.6) for $\bar{\sigma}$.

References

[1] L.D. Landau and I.Y. Pomeranchuk, Dokl. Akad. Nauk SSSR 102 (1955) 489;
E.S. Fradkin, Sov. Phys. JETP 28 (1955) 750
[2] M. Gell-Mann and F. Low, Phys. Rev. 95 (1954) 1300;
K. Symanzik, Commun. Math. Phys. 18 (1970) 227;
C.G. Callan, Phys. Rev. D2 (1970) 1541
[3] J.B. Kogut, E. Dagotto and A. Kocic, Phys. Rev. Lett. 60 (1988) 772
[4] J.B. Kogut, E. Dagotto and A. Kocic, Nucl. Phys. B317 (1989) 253
[5] J.B. Kogut, E. Dagotto and A. Kocic, Nucl. Phys. B317 (1989) 271
[6] J.B. Kogut and E. Dagotto, Phys. Rev. Lett. 59 (1987) 617;
H.C. Hege and A. Nakamura, Nucl. Phys. B (Proc. Suppl.) 9 (1989) 114
[7] M. Okawa, Phys. Rev. Lett. 62 (1989) 1224
[8] S.P. Booth, R.D. Kenway and B.J. Pendleton, Phys. Lett. B228 (1989) 115
[9] E. Dagotto, A. Kocic and J.B. Kogut, Illinois preprint ILL-(TH)-89-34 (1989)
[10] V.A. Miransky, Nuovo Cimento 90A (1985) 149; Sov. Phys. JETP 61 (1985) 905;
P.I. Fomin, V.P. Gusynin, V.A. Miransky and Yu.A. Sitenko, Riv. Nuovo Cimento 6 (1983) 1
[11] I. Barbour, *in*: Proc. Gauge theory on a lattice (Argonne, 1984);
G. Schierholz, *in*: Fundamental forces, ed. D. Frame and K.J. Peach, Scottish Universities Summer School in Physics Publications (Edinburgh, 1985)
[12] T. Jolicoeur and A. Morel, Nucl. Phys. B262 (1985) 627
[13] A. Morel, Saclay preprint PhT/87-020 (1987)
[14] J. Gasser and H. Leutwyler, Phys. Lett. B188 (1987) 477
[15] M. Abramowitz and I.A. Stegun, Handbook of Mathematical Functions (Dover, New York, 1965)
[16] N. Kawamoto and J. Smit, Nucl. Phys. B192 (1981) 100
[17] S.-K. Ma, Modern theory of critical phenomena (Benjamin, Reading, 1976)
[18] I.M. Barbour, N.-E. Behill, P.E. Gibbs, G. Schierholz and M. Teper, *in*: The recursion method and its applications, ed. D.G. Pettifor and D.L. Weaire (Springer, Berlin, 1985) p. 149
[19] S. Duane, A.D. Kennedy, B.J. Pendleton and D. Roweth, Phys. Lett. B195 (1987) 216

[20] K. Bitar, A.D. Kennedy, R. Horsley, S. Meyer and P. Rossi, Nucl. Phys. B313 (1989) 348, 377;
R. Gupta, G. Kilcup and S. Sharpe, Phys. Rev. D38 (1988) 1278;
R. Gupta, A. Patel, C. Baillie, G. Guralnik, G. Kilcup and S. Sharpe, Phys. Rev. D40 (1989) 2072
[21] A. Horowitz, talk at the Int. Workshop Lattice 89, Capri, September 1989; Phys. Lett. B219 (1989) 329
[22] I.-H. Lee and R.E. Shrock, Phys. Rev. Lett. 59 (1987) 14